Contrail Altitude Estimation Based on Shadows Detected in Landsat Imagery

Roosenbrand, E.J.; Sun, Junzi; Hoekstra, J.M.

Publication date
2023

Document Version
Submitted manuscript

Citation (APA)
Roosenbrand, E. J., Sun, J., & Hoekstra, J. M. (2023). *Contrail Altitude Estimation Based on Shadows Detected in Landsat Imagery*. Paper presented at 13th SESAR Innovation Days, Sevilla, Spain.

Contrail Altitude Estimation Based on Shadows Detected in Landsat Imagery

Esther Roosenbrand, Junzi Sun, Jacco Hoekstra
Control and Simulation, Faculty of Aerospace Engineering
Delft University of Technology, The Netherlands

***Abstract*—Contrails contribute to global warming by trapping outgoing terrestrial radiation, exerting an immediate warming influence on the climate. The climatic impact of contrails is potentially comparable to that of aviation's carbon emissions. This underlines the importance of minimizing contrail formation to mitigate the climate effects of aviation, both now and in the future. The evaluation of contrails demands more precise data on the location and altitude where they form. Remote sensing imagery enables the identification of their location. Nevertheless, determining the altitude of the contrail remains problematic, complicating the identification of the source flight. This study introduces a novel method that enables researchers to determine the altitude of a contrail solely using Landsat data by analysing shadows cast by contrails. Through validation against ADS-B data from OpenSky, we demonstrate that such a technique can achieve the accuracy of a few hundreds of meters, which is suitable for incorporation into a climate-optimized routing system. Finally, a ResUNet segmentation model is also presented, which can identify contrails and their shadows in Landsat imagery. These results constitute a step forward for more accurate contrail dataset and models.**

***Keywords*—Sustainability, Contrails, Remote Sensing, Atmospheric Science, OpenSky, Aircraft Surveillance Data**

I. Introduction

With the number of flights continuing to rise globally, aviation's climate impact is also growing, making sustainability one of the biggest challenges facing the aerospace industry today. The most significant individual contributor to aviation's total radiative forcing at shorter timescale is the formation of contrail cirrus, albeit with some uncertainties [1]. While carbon dioxide emissions today influence global warming on a timescale of 20–40 years, the warming effect of contrails is immediate [2]. This emphasizes the importance of minimizing contrail formation as a means to promptly limit aviation's climate impact and secure a sustainable future.

The successful implementation of a climate-optimized routing system [3], designed to avoid contrail formation, hinges on an adequate understanding of the atmospheric conditions conducive to either the formation or absence of contrails. The aircraft's altitude is a crucial factor. To achieve this, knowing the location and more importantly the altitude at which the contrails form are essential, as this dictates the atmospheric conditions allowing for contrail formation. Knowledge of these atmospheric conditions will allow for creation of a climate-optimized routing system.

While remote sensing-based methods for determining atmospheric conditions through contrail location (including its altitude) have proven effective in quiet airspace [4], a robust model, as described above, necessitates a larger dataset for training. This would entail the challenging task of linking contrails observed in infrared imagery to flight data, such as ADS-B [5], [6], to extract contrail-forming atmospheric conditions. This is why a methodology to determine contrail forming altitudes, that does not require the assignment of flight trajectories to contrails, namely through shadow detection, will be explored here.

In the remote sensing field, shadow detection is an essential data processing step to ensure the quality of satellite images, which are often partially obscured by clouds. Clouded and shadowed imagery complicates the use of optical Earth observation satellites, as they cause a brightening and darkening effect, respectively [7]. These can be seen in Figure 1, a true-color image illustrating a contrail, its associated shadow, and cirrus clouds in the upper left corner.

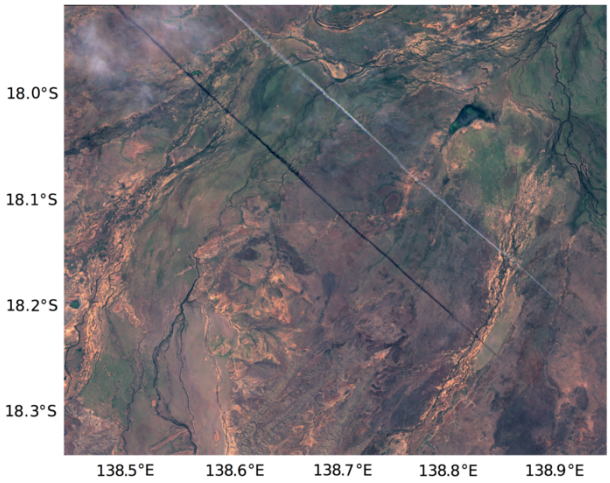

Figure 1. LANDSAT 8 True Colour RGB on April 4th 2017, West Queensland in Australia, with contrail visible as white diagonal stripe and the shadow it casts above to the South.

Using shadow locations as a determination of cloud height is commonly applied in the determination of plume heights of volcanic eruptions, which is an important parameter for dispersal dynamics and their eruption intensity [8]. By using the shadows cast on the Earth's surface and solar geometry, plume or cloud heights can be determined, as demonstrated in Figure 2.

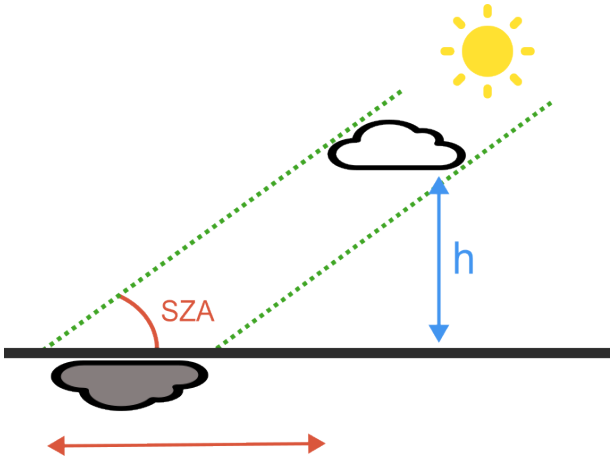

Figure 2. Sun and cloud (shadow) geometry, with indications of the solar zenith angle (SZA), the ground distance (horizontal red arrow) and the cloud height (blue arrow *h*). To summarize: h = cos(SZA) * ground distance

Traditionally, this shadow method is often performed manually and for one volcano at a time. Besides this being time-consuming for a large amount of contrails, contrail detection requires identifying linear features, a task that could rely on computer vision techniques [5].

Fully utilizing the recent advancements in this field, this paper presents a U-Net segmentation model, which was trained to detect both contrails and their shadows.

Subsequently, using the methodology outlined in Figure 2, the contrail and aircraft altitudes are determined. These altitudes are validated against ADS-B flight data from OpenSky, gauging the methodology's precision and suitability for integration into a climate-optimized routing system.

Once local altitude specific atmospheric data has been incorporated into these contrail forming flights, this atmospheric dataset will form the basis of a future climate-optimized routing model, which could then be incorporated into ATC planning similarly to a weather forecast.

The paper is organized as follows: it begins with an introduction to the open-source data used. Following that, the methodology is explained, along with an overview of the ResUNet's structure. The subsequent sections present the validation results and the outcomes of the ResUNet model, followed by a discussion of these results. The paper concludes with a summary of key findings.

II. Data

A. LANDSAT 8

We obtained LANDSAT 8 imagery using the sat-search STAC API[1], which provides access to NASA's Earth Observing System Data and Information System (EOSDIS) services. The Landsat 8 satellite operates in a sun-synchronous orbit with a 10:00 AM local time equator-crossing overpass, capturing data for every point on Earth approximately once every 16 days.

[1]https://github.com/sat-utils/sat-search, (last access: November 21, 2023)

TABLE I: LANDSAT 8 BANDS CHARACTERISTICS

Bands	**Wavelengths (µm)**	**Spatial Resolution (m)**
Band 1: Coastal Aerosol	0.43 - 0.45	30
Band 2: Blue	0.45 - 0.51	30
Band 3: Green	0.53 - 0.59	30
Band 4: Red	0.64 - 0.67	30
Band 5: NIR	0.85 - 0.88	30
Band 6: SWIR 1	1.57 - 1.65	30
Band 7: SWIR 2	2.11 - 2.29	30
Band 8: Panchromatic	0.50 - 0.68	15
Band 9: Cirrus	1.36 - 1.38	30
Band 10: Thermal Infrared 1	10.6 - 11.19	100
Band 11: Thermal Infrared 2	11.5 - 12.51	100

LANDSAT 8 offers 11 bands with varying wavelengths and spatial resolutions, as detailed in Table I. Besides these bands, the QA (Quality Assessment) band was also downloaded, which represents the usefulness of each pixel. The QA band is primarily used to filter out pixels with cloud cover, based on tests on the spectral bands in Table I. Besides (cirrus) cloud, snow and ice cover, water pixels are also identified. This QA water filter was applied, since during the initial training of the model, it became apparent that rivers were incorrectly identified as contrail shadows.

When downloading through the EOSDIS services, *.tif* files for each of the bands in Table I are collected, as well as the metadata file containing the geographic extent, sensing time, and the solar zenith angle of the Landsat images.

B. ADS-B data from OpenSky

The OpenSky Network has been collecting global air traffic surveillance data since 2013, including unfiltered and raw data from ADS-B, Mode S, TCAS, and FLARM messages [9]. The geoaltitude from the GNSS (GPS) sensor onboard the aircraft is used as validation value for the altitude determined through the shadow-contrail distance. However, geoaltitude indicates the vertical distance of an aircraft from a reference ellipsoid indicating sea level. To correct this, an elevation correction is applied.

ADS-B data from OpenSky was used to manually validate the calculated contrail altitudes of the detected contrail-shadow pairs. Only cases were used where the risk of incorrect flight track to contrail assignment was minimal (unique flight tracks or uncrowded airspace). This left 56 labelled flights.

III. Method

In this section, the models and methods used to determine contrail altitude based on their shadows are discussed.

A. Identifying contrails and their shadows

Contrails are not easily identifiable from unprocessed satellite data, since a contrail can be just a few meters wide [10], can be similar in appearance to cirrus clouds and be somewhat transparent in RGB imagery.

On the other hand, contrail's linear geometry can help in differentiating them from the background. Contrails and cirrus clouds are atmospherically similar, so infrared channels which

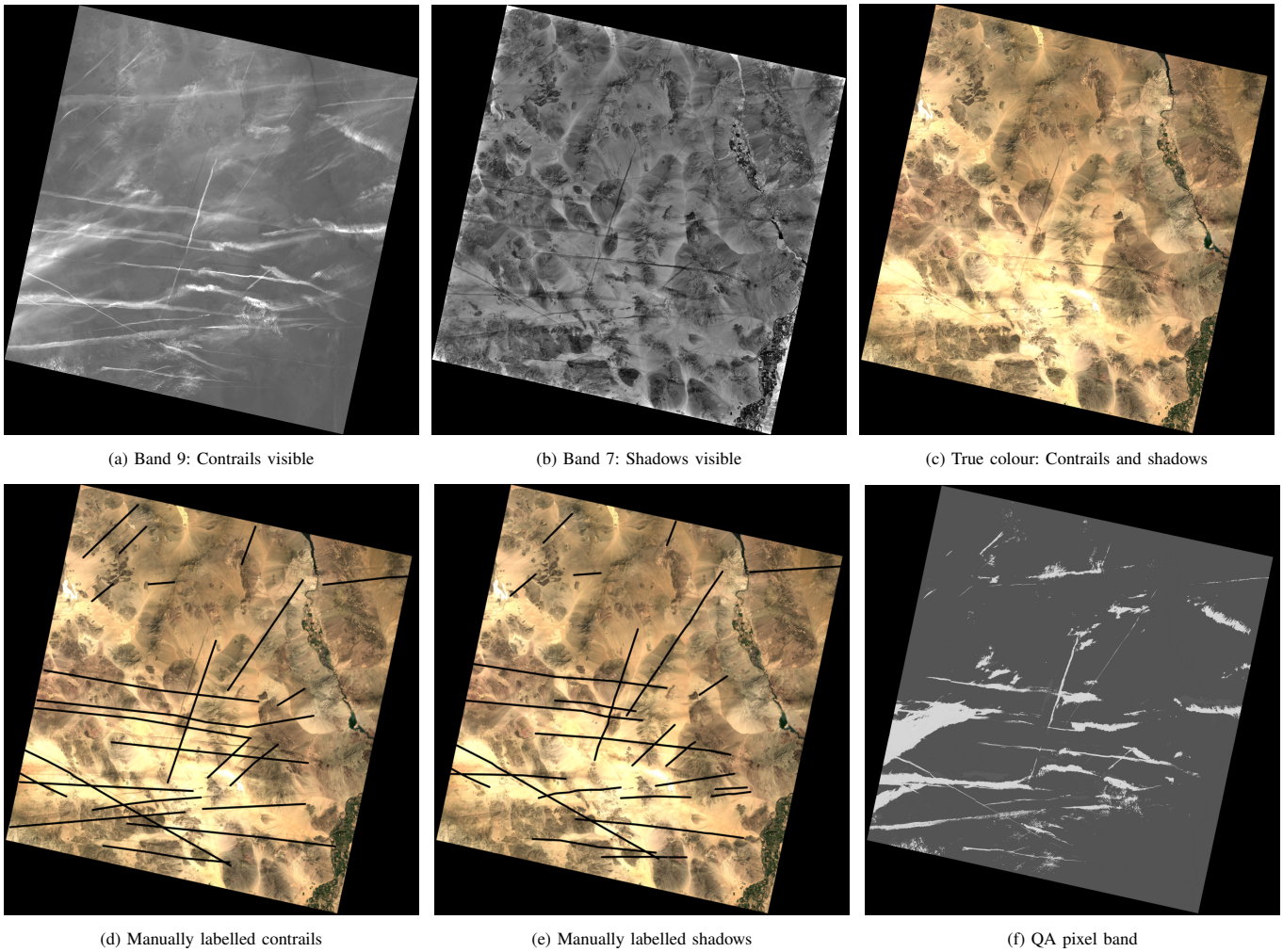

(a) Band 9: Contrails visible

(b) Band 7: Shadows visible

(c) True colour: Contrails and shadows

(d) Manually labelled contrails

(e) Manually labelled shadows

(f) QA pixel band

Figure 3. Six Landsat 8 images from March 3rd 2015, near Joshua Tree National Park, California, USA. The images are rotated so north is towards the top of the image. The scene size of each image is 185x180 km.

are used to identify cirrus clouds can also be used to detect contrails.

The identification and labelling of shadows also relies on a similar linear feature. However, it is more challenging as the background impacts shadow detection more significantly than with contrails. This difference in background impact is clearly visible in comparing Figure 3 (a) with (b). We determined shadow locations based on true-colour RGB images and Band 7, because cloud shadow scattering is strongest in the short wavelengths, such as SWIR (short-wave infrared) [11].

The manual labelling was done in GIMP, which is an open-source raster graphic editor. It allows for efficient switching between image layers, while maintaining alignment. The individual bands were normalized and by using GIMP's shadow/highlight tool the contrast within an image was increased, to make the labelling easier. Once two vector sets were drawn, one indicating contrails and another for shadows, these vectors were mapped onto an empty raster layer, with a stroke of 20pt.

In Figure 3, six Landsat images are shown, in (a), (b), (c) and (f) the images used in the labelling process, and in (d) and (e) the resulting labelled images for the contrail and the shadows.

B. Determining shadow distance with Hough transformation

Our objective is to find the pairs of contrail and shadow that belong to each other, calculate the distance between the pair, and then apply the principle sketched in Figure 2 to determine the altitude of the contrails.

In Figure 3. (d) and (e), we can see that the contrail and shadow are shifted in location, but the lines are essentially parallel. This angle similarity and a shift in distance will be exploited to pair the two together, by using the Hough Transform [12].

The Hough transformation allows lines from the Cartesian coordinate system to be presented as points in a polar coordinate system, where the similar angular values in the Hough space indicates that the original lines are parallel. Furthermore, for parallel lines in Cartesian system, their distance can also be calculated easily in the Hough space.

The Hough Transform maps patterns to a parameter space, meaning that a line ($y = ax + b$) in the image space (x-y) represents a point in the parameter space ($\rho = x\cos(\theta) + y\sin(\theta)$). ρ is the distance from the origin to the closest point on the line, and θ the angle between the horizontal axis and the new line. This is visualized in Figure 4.

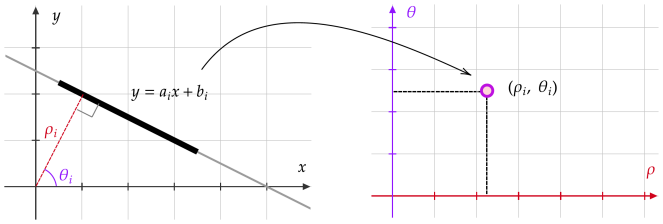

Figure 4. Example of Hough transform

Each contrail and shadow line was represented as a point in the parameter space, as illustrated in Figure 5. The proximity between these points indicated similarities in their slopes and spatial closeness, as shown in Figure 5.

After associating each shadow with a contrail, the orthogonal distance between these two lines is calculated as the difference in the distance from the origin to the closest point on each straight line (ρ (rho) in the parameter space). The unit of this distance is pixels, which can be converted into meters by multiplying it by 30 (the grid cell size of Landsat's thermal imagery).

C. Calculate contrail altitude

In order to ensure this ground distance from contrail to shadow is orthogonal, a correction was applied based on the sun's azimuth. The Sun's position as relative to an observer on the Earth surface is determined by the azimuth and zenith angles. The zenith angle is indicated as SZA in Figure 2, and is the vertical angular distance between the Sun and the horizontal plane. The azimuth angle is the angular distance measured clockwise from directly north.

$$\text{contrial altitude} = \frac{\text{hough distance}}{sin(\text{sun azimuth} - \Delta\theta))} * tan(\text{SZA}))$$

D. Neural network model for contrail and shadow detection

In this research, we continue our earlier work on a ResUNet neural network model for contrail detection [5], and adapt it for detecting both contrails and shadows with the manually labelled data. The open-source model from [5] has previously proven to be highly effective in handling varied image quality, including contrast, distortions, and lighting conditions. The customized SR Loss function is also effective in identifying the linear feature line contrails and shadows.

The ResUNet model used in this study combines the U-Net and ResNet architecture. A U-Net is a convolutional neural network, that includes encoder and decoder paths. The encoder captures the input image's features by progressively reducing dimensions and increasing depth. The decoder uses up-sampling with transposed convolutions for pixel-wise segmentation, restoring the spatial resolution.

U-Net is commonly incorporated with ResNet, a type of network designed to address the challenge of the diminishing gradients in neural network training. When combined, the mode contains U-Net with ResNet encoder (ResUNet), where the ResNet acts as the backbone for feature extraction, and U-Net acts as the decoder for segmentation. The model detail can be found in [5].

To train the models, 55 images were selected from locations around the world and manually labeled for contrails and their shadows. Once the Landsat data has been labeled, the pre-trained U-Net segmentation model is applied.

The model is trained on 34 labeled images, and 21 used for validation. Splitting the data in training and testing was done so that both groups included a variation in contrail interplay (from parallel to crossing tracks). It was also ensured that all validation images had OpenSky coverage.

Traditionally, 34 images is a relatively small data set to use in neural network training. However, image augmentation [13] is applied at each training step to a random selected batch of images. This allows the model to become more generalized from only a limited number of manually labeled images [5].

Before inputting the satellite images into the network model, we normalized each individual band image. Contrail and shadow detection were trained separately.

One of the main ground features that can confuse the neural network model is rivers. The QA band from Landsat can be used to identify areas of water. In the pre-processing of the input imagery, we replace the pixel values in these areas with values from the background. Fortunately, roads, power lines and other dark man-made linear features were typically too thin to be mistaken for shadows or contrails.

IV. Analysis & Results

The methodology presented in the previous section will be evaluated against aircraft GPS's altitude here. First, however, the results of the coupling of the contrail and shadow pairs are shown.

A. Calculated Altitudes

Based on this methodology, we computed the *'calculated altitude'* values presented in Table II. Subsequently, we associated the contrails with OpenSky trajectories, obtaining the ICAO24 codes and geoaltitudes. Pair 3 from Fig. 5 is not considered because the OpenSky counterpart could not be established with sufficient certainty.

TABLE II: SHADOW ALTITUDE COMPARED WITH OPENSKY

Pair number	Aircraft icao24	Calculated altitude	Aircraft GPS altitude
0	ab4e94	12.446	12.137
1	a213bd	9.979	10.043
2	a448f8	10.003	10.356

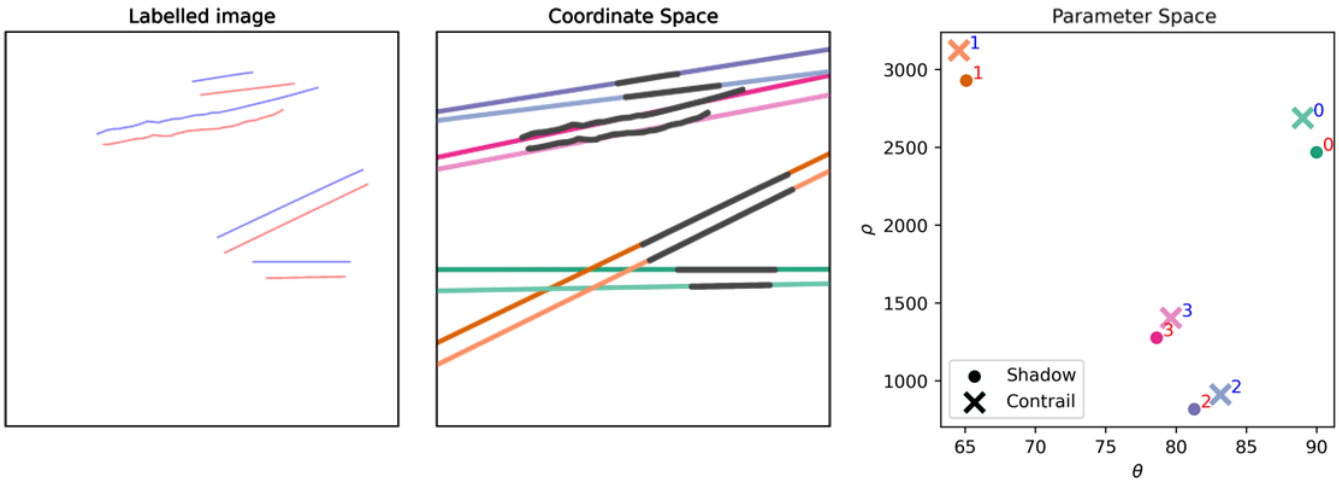

Figure 5. Hough Transform, the first image shows the labelled contrail (red) and shadow (blue) lines, the second the detected Hough lines, in the third image each of these lines in the coordinate space is represented by a point in the parameter space. The numbers near each point indicate the pair formed.

Table II, shows the results for a single set of Landsat images, this methodology was subsequently repeated for all 55 images sets. All of these differences between the calculated altitudes and aircraft GPS altitude pairs (as shown in Table II) are presented in the top histogram in Figure 6. These altitude differences exhibit a normal distribution centred around zero.

In the lower histogram in Figure 6, we see the relative altitude difference as compared with OpenSky data, which shows a range of maximum 7% for an average aircraft GPS altitude of 11.263 meters and average calculated altitude of 11.433 meters over 44 flights.

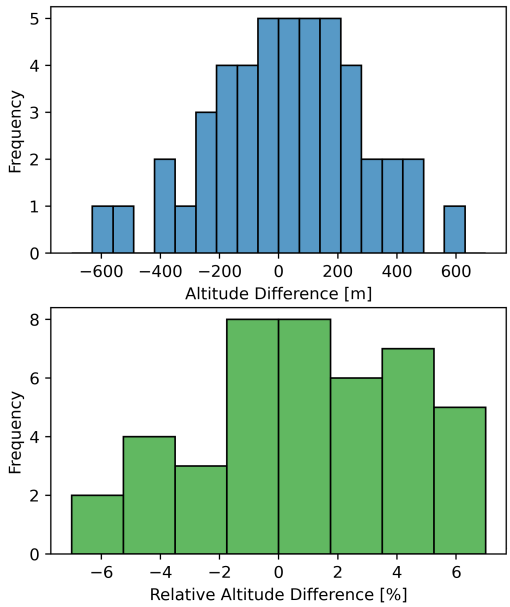

Figure 6. Histogram of altitude differences between aircraft GPS altitude and the calculated altitude based on shadow distances for all 44 flights considered. The top histogram shows the altitude difference, while the bottom shows the relative altitude difference with the aircraft GPS altitude.

As expected, outliers occur when significant elevation differences occur in the terrain. Another reason for the outliers are large differences between the theta's of pairs. In the Hough space, this implies that the lines in a pair might be near, but their angles are different. Visual inspections of the large difference cases confirmed the contrail-shadow pairs were correct, but in many cases, the shadow starts parallel to the contrail and then bends away or towards it.

This most likely implies a climbing or descending aircraft, and so causes an error both in the aircraft GPS altitude and the calculated altitude. For this reason, pairs where the theta difference was larger than 2 were also eliminated from the histogram in Figure 6.

B. Contrails and shadows detection from neural networks

To assess the efficiency of detecting contrails and shadows based on our previously proposed ResUNet neural network models, the performance is evaluated based on images unused in training. The neural network model is trained with 4000 steps (around 1500 epochs).

Figure 7 shows a few examples of how the contrail detection model performs on images from in the testing set. The first column shows the image used for testing the ResUNet, the second column displays manually labeled contrails and shadows, and the third column reveals the contrail predictions generated by the ResUNet. We can observe a high accuracy for contrail detection model.

The shadow detection is not as accurate as the contrail detection. This model is trained for 9000 steps (around 3000 epochs). Figure 8 shows a few examples to illustrate the performance of shadow detection ResUNet, where it becomes apparent that the main challenge is the ground features.

The model has difficulties to distinguish between linear ground features and shadows. It only performs well when backgrounds are relatively uniform, as shown in the first two plots. However, in the third plot, the dark ground features are identified as shadows.

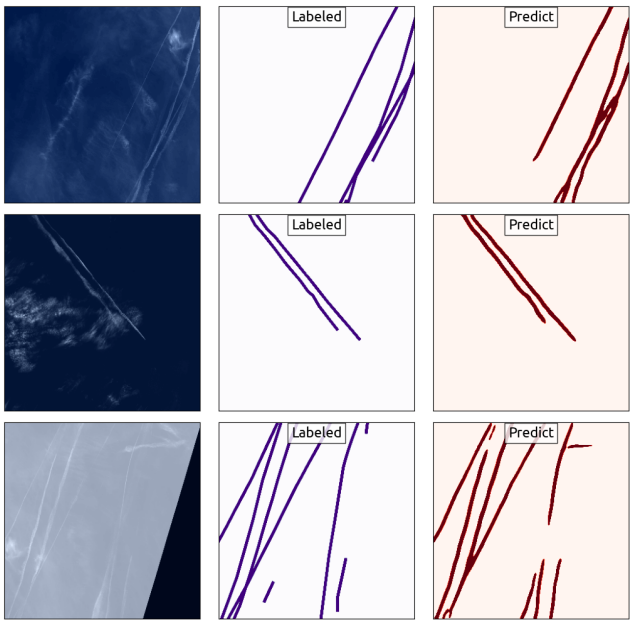

Figure 7. Application of the contrail detection ResUNet model with unseen Landsat images, next to the labelled contrail images and the results of the ResUNet.

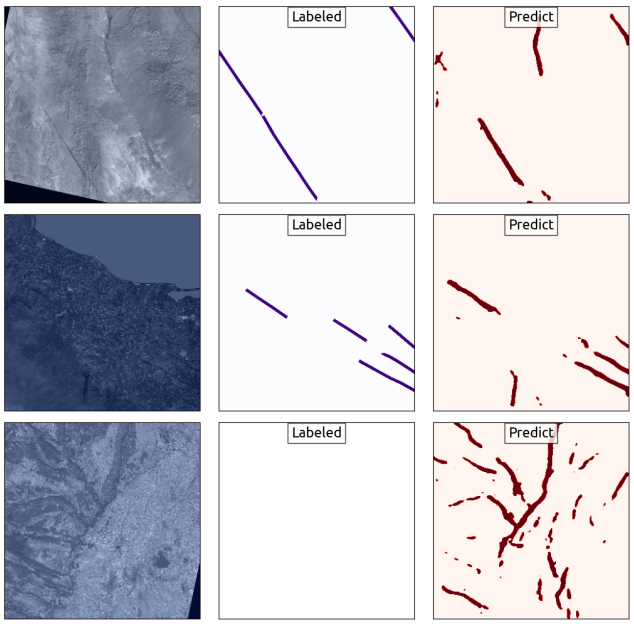

Figure 8. Application of the shadow detection ResUNet model with unseen Landsat images, next to the labelled shadow images and the results of the ResUNet. The last image shows the model in the case where there is no shadow present.

It is worth noting that the performance of contrail and shadow model during the trainings are also different. In Figure 9, we show the intersection over union (IoU), a common metric to evaluate object detection performance, during the two training processes. The top and bottom plots show the IoU improvement for training and validation datasets, respectively.

It can be observed that the contrail model learns quickly, and reaches a much higher accuracy than the shadow model. The shadow model has a very shallow learning curve with much lower accuracy.

However, based on the trends from both curves, we think improvement could still be made with more epochs. We suspect that the model for shadow detection may require a significantly longer training with the ResUNet model. A model with more parameters or a different neural net model architecture shall also be tested to improve the shadow detection model. In the follow-up research, our aim is to achieve a similar level of performance as the contrail detection.

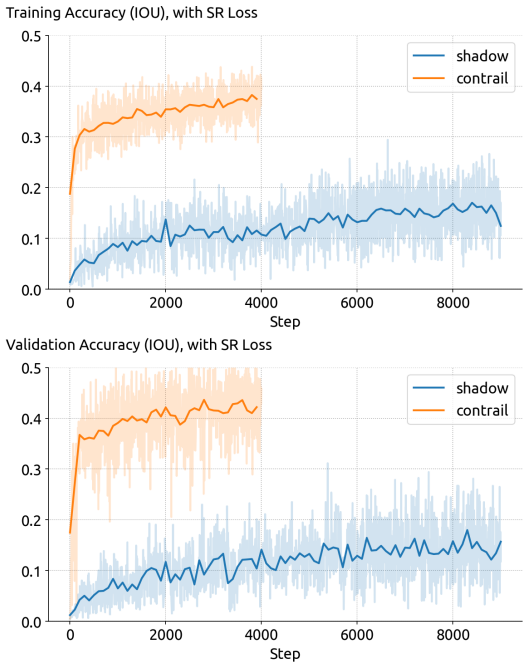

Figure 9. Training and validation errors during training and validating for both the contrail and shadow detection model. The contrail model learns quickly, and reaches a much higher accuracy than the shadow model.

V. Discussion

A. Required Accuracy

The reason behind determining contrail formation altitudes is the creation of a climate-optimized routing system based on atmospheric conditions. This entails linking contrail formation altitudes and atmospheric datasets, such as ECMWF's (European Centre for Medium-Range Weather Forecasts) ERA5 Atmospheric Reanalysis [6], [14], or NOAA's (United States National Oceanic and Atmospheric Administration) Rapid Updated Cycle [15], [16].

Both of these datasets are supplied on 37 pressure levels from 1000 hPa to 1 hPa, with a typical step size of 25 hPa. This resolution is around 800 m (2625 feet), which is well within the typical error of the altitude differences presented in Figure 6, and so our methodology provides an altitude estimation that falls within the required accuracy for contrail avoidance.

In this paper, the geoaltitude from OpenSky ADS-B is taken as a ground truth, as the benchmark to measure the shadow

determined altitude against. This has proven to be an accurate methodology of determining flight levels [17].

B. Landsat Scenes

The methodology presented in this paper focuses on flat terrain, because correcting for shadow distortions caused by topography effects was considered beyond the scope of this study. However, extensive research is available on how to incorporate digital elevation models into the prediction from volcanic research [8], [18].

Besides the bands shown in Table I, a QA pixel file is also included with the Landsat data. This mask layer identifies pixels that are likely covered by clouds, shadows or contain water. This mask is based on the object-based Fmask [19]. While the mask does include prediction for both clouds and shadows, we have observed that in many cases the contrails and their shadows are probably too thin to be predicted by the Fmask.

While the assignment of flight trajectories to individual contrails, as demonstrated in previous studies [5], [6], presents challenges, the advantage is that the aircraft-type is acquired. This will ultimately be necessary to obtain when the climate optimal route is determined, since the aircraft engine and the flight level limitations should be considered [20].

C. Improvements to ResUNet

Questions about required accuracy also arise when discussing the ResUNet, where 100% detection is not necessary. The caveat being that contrails and shadow pairs being missed, do not exhibit any bias. The purpose of the ResUNet is to create an inventory of contrail forming conditions, not necessarily to detect every possible contrail-shadow pair.

Nevertheless, improvements can and arguably should still be made based on Figure 9, especially for the shadow detection, where the IOU graph plateaus around 17%. To achieve these improvements, change detection in the time series of satellite images [21] could be used. First, a cloud-free image with the same spatial coverage, which was gathered around a similar time as the original image, is downloaded, and subsequently this cloud-free image is subtracted from the contrail image. The difference between these images should highlight shadows in Band 7 and the contrails in Band 9. Training the model on these images, instead of the regular ones, could improve the contrail and shadow detection.

Additionally, both older and younger contrails were labelled in this work. In some cases, the contrails were so young that the aircraft was still visible in the Landsat image. Young contrails often remain clearly visible in RGB true-color images and Band 11, but their shadows may not exhibit the necessary contrast for accurate detection in Band 7. As contrails age, they become more diffuse and spread out horizontally. This makes detecting the contrails and their shadows easier, but care should be taken to label them correctly in the centre of the contrail, otherwise the methodology illustrated in Figure 2 will fail.

Another consideration for only labelling younger contrails is that there is more assurance that the altitude calculated is the contrail *formation* altitude. This can be different from the contrail *presence* altitude, because there has been little time to vertically displace the contrail, because of a dynamic atmosphere.

Because of the limited temporal resolution of Landsat imagery (revisit time of 16 days) determining the persistence of the detected contrails is a challenge. As the persistence of contrails is an important climate metric, this could be mitigated by incorporating geo-stationary satellite imagery (as in [6]), once the contrail has been detected and the altitude has been calculated.

Future work will involve further improvements to the ResUNet model as described above, as well as incorporating ECMWF ERA-5 Reanalysis data (and potentially IGRA weather balloon data) to construct a contrail forming atmospheric conditions model. This model could then act similarly to a weather forecast, with the ATC planning of the route.

VI. Conclusion

This study introduces a novel method for determining contrail altitudes from their shadows using only the Landsat imagery. The methodology outlined in this study accomplishes a pivotal milestone by accurately determining contrail formation altitudes. It provides contrail altitudes with an accuracy suitable for integration into climate-optimized flight planning systems. This paves the way for practical contrail avoidance measures that can be employed in flight operations, contributing to the overall reduction in aviation's climate impact.

A neural network segmentation model is also presented, which allows for the automatic detection of contrail and their corresponding shadows. With further enhancement, this model can be used to produce a consistent contrail dataset useful for validating existing and future contrail models. It also expands the scope of machine learning applications in contrail detection and environmental monitoring via satellite imagery.

Overall, the contributions of this study not only fill a current gap in contrail research but also set the stage for future innovations in the field of contrail assessment.

VII. Source Code and Additional Results

The source code and data are available at:
https://github.com/junzis/contrail-net.

Acknowledgements

The project is partially funded by the TU Delft Climate Action Seed Fund Grants. We would also like to extend our thanks to David Paredes and Josep Pino for hosting Esther at Aistech Space and for their support of this research.

References

[1] V. Grewe, K. Dahlmann, J. Flink, C. Frömming, R. Ghosh, K. Gierens, R. Heller, J. Hendricks, P. Jöckel, S. Kaufmann *et al.*, "Mitigating the climate impact from aviation: Achievements and results of the dlr wecare project," *Aerospace*, vol. 4, no. 3, p. 34, 2017.

[2] D. Avila, L. Sherry, and T. Thompson, "Reducing global warming by airline contrail avoidance: A case study of annual benefits for the contiguous united states." *Transportation Research Interdisciplinary Perspectives*, vol. 2, 2019.

[3] E. Roosenbrand, J. Sun, I. Dedoussi, D. Stam, and J. Hoekstra, "Assessing and modelling climate optimal flightsusing open surveillance and remote sensing data." *ICRAT 2022*, 2022.

[4] E. Roosenbrand, J. Sun, and J. Hoekstra, "Examining contrail formation models with open flight and remote sensing data." *SIDS 2022*, 12 2022.

[5] J. Sun and E. Roosenbrand, "Contrail segmentation using augmented transfer learning with a novel loss function in hough space," 2023. [Online]. Available: https://arxiv.org/pdf/2307.12032.pdf

[6] R. Chevallier, M. Shapiro, Z. Engberg, M. Soler, and D. Delahaye, "Linear contrails detection, tracking and matching with aircraft using geostationary satellite and air traffic data," *Aerospace*, vol. 10, no. 7, 2023.

[7] Z. Zhu and C. Woodcock, "Object-based cloud and cloud shadow detection in landsat imagery," *Remote Sensing of Environment*, vol. 118, p. 83–94, 03 2012.

[8] S. Pailot-Bonnétat, A. J. L. Harris, S. Calvari, M. De Michele, and L. Gurioli, "Plume height time-series retrieval using shadow in single spatial resolution satellite images," *Remote Sensing*, vol. 12, no. 23, 2020. [Online]. Available: https://www.mdpi.com/2072-4292/12/23/3951

[9] M. Strohmeier, O. Xavier, L. Jannis, M. Schäfer, and V. Lenders, "Crowdsourced air traffic data from the opensky network 2019–2020." *Journal of Air Transport Management*, vol. 94, 2021.

[10] U. Schumann, R. Baumann, D. Baumgardner, S. T. Bedka, D. P. Duda, V. Freudenthaler, J.-F. Gayet, A. J. Heymsfield, P. Minnis, M. Quante, E. Raschke, H. Schlager, M. Vázquez-Navarro, C. Voigt, and Z. Wang, "Properties of individual contrails: a compilation of observations and some comparisons," *Atmospheric Chemistry and Physics*, vol. 17, no. 1, pp. 403–438, 2017.

[11] Y. Luo, A. Trishchenko, and K. Khlopenkov, "Developing clear-sky, cloud and cloud shadow mask for producing clear-sky composites at 250-meter spatial resolution for the seven modis land bands over canada and north america," *Remote Sensing of Environment - REMOTE SENS ENVIRON*, vol. 112, pp. 4167–4185, 12 2008.

[12] P. V. C. Hough, ""method and means for recognizing complex patterns," Ser. No. 17,7156 Claims 3,069,654.

[13] A. Buslaev, V. I. Iglovikov, E. Khvedchenya, A. Parinov, M. Druzhinin, and A. A. Kalinin, "Albumentations: Fast and flexible image augmentations," *Information*, vol. 11, no. 2, 2020.

[14] R. Teoh, U. Schumann, and M. E. J. Stettler, "Beyond contrail avoidance: Efficacy of flight altitude changes to minimise contrail climate forcing," *Aerospace*, vol. 7, no. 9, 2020.

[15] N. Chen, B. Sridhar, and H. Ng, "Tradeoff between contrail reduction and emissions in united states national airspace," *Journal of Aircraft*, vol. 49, pp. 1367–1375, 09 2012.

[16] B. Sridhar, N. Y. Chen, and H. K. Ng, "29th digital avionics systems conference," pp. 1.A.1–1–1.A.1–9, 2010.

[17] B. S. Ali and N. A. Taib, "A study on geometric and barometric altitude data in automatic dependent surveillance broadcast (ads-b) messages," *The Journal of Navigation*, vol. 72, no. 5, pp. 1140–1158, 2019.

[18] S. Qiu, B. He, Z. Zhu, Z. Liao, and X. Quan, "Improving fmask cloud and cloud shadow detection in mountainous area for landsats 4–8 images," *Remote Sensing of Environment*, vol. 199, pp. 107–119, 09 2017.

[19] Z. Zhu, S. Wang, and C. E. Woodcock, "Improvement and expansion of the fmask algorithm: cloud, cloud shadow, and snow detection for landsats 4–7, 8, and sentinel 2 images," *Remote Sensing of Environment*, vol. 159, pp. 269–277, 2015.

[20] K. Radhakrishnan, K. Deck, P. Proesmans, F. Linke, F. Yin, V. Grewe, R. Vos, B. Lührs, M. Niklaβ, and I. Dedoussi, "Minimizing the climate impact of the next generation aircraft using novel climate functions for aircraft design," in *ICAS PROCEEDINGS 33th Congress of the International Council of the Aeronautical Sciences*, 2022.

[21] T. Zhou, H. Fu, C. Sun, and S. Wang, "Shadow detection and compensation from remote sensing images under complex urban conditions," *Remote Sensing*, vol. 13, no. 4, 2021.